SUPPORTING INFORMATION

Concomitant Emergence of Circularly Polarized Luminescence and Single-Molecule Magnet Behavior in Chiral-at-Metal Dy Complex

Bahjat El Rez,[a] Jiawen Liu,[c] Virginie Béreau,[a,b] Carine Duhayon,[a] Yuki Horino,[d] Takayoshi Suzuki,[d,e] Laurent Coolen,*[,c] Jean-Pascal Sutter*[,a]

[a] Laboratoire de Chimie de Coordination du CNRS (LCC-CNRS), Université de Toulouse, CNRS, Toulouse, France
sutter@lcc-toulouse.fr
[b] Université de Toulouse, Institut Universitaire de Technologie-Département de Chimie, Castres, France
[c] Sorbonne Université, CNRS, Institut de NanoSciences de Paris, INSP, F-75005 Paris, France
coolen@insp.jussieu.fr
[d] Graduate School of Natural Science and Technology, Okayama University, Okayama 700-8530, Japan.
[e] Research Institute for Interdisciplinary Science (RIIS), Okayama University, Okayama 700-8530, Japan

CONTENTS

Picture 1. Crystals of [L^{Me2}Zn(Cl)Dy(*(-)*-camph)$_2$(MeOH)], **Δ-Dy**.

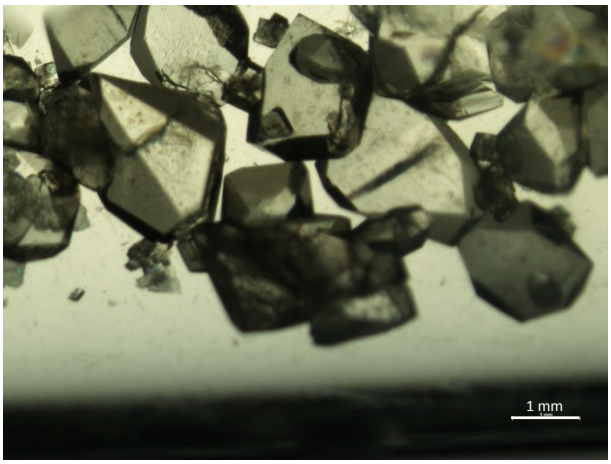

Table S1. Crystal data for **Λ-Dy**, **Δ-Dy**, **Λ-Eu,** and **Λ-Dy/Y**.

Compound	**Λ-Dy**	**Δ-Dy**	**Λ-Eu**	**Λ–Dy/Y**
Empirical formula	$C_{46}H_{56}ClDyF_6N_2O_9Zn$	$C_{46}H_{56}ClDyF_6N_2O_9Zn$	$C_{46}H_{56}ClEuF_6N_2O_9Zn$	$C_{46}H_{56}ClDy_{0.16}F_6N_2O_9Y_{0.84}Zn$
Formula weight (g·mol^{-1})	1158.28	1158.28	1147.74	1096.46
λ (Å)	0.71073	0.71073	1.54180	0.71073
Temperature (K)	100	100	100	110
Crystal system	Orthorhombic	Orthorhombic	Orthorhombic	Orthorhombic
Space group	*P* 2_1 2_1 2_1	*P* 2_1 2_1 2_1	*P* 2_1 2_1 2_1	*P* 2_1 2_1 2_1
a (Å)	13.0607(9)	13.0364(7)	13.0430(2)	13.0472(5)
b (Å)	18.8726(11)	18.8572(11)	18.9020(2)	18.8726(7)
c (Å)	19.3077(13)	19.2842(11)	19.3871(2)	19.2735(9)
Volume (Å^3)	4759.1(5)	4740.6(3)	4779.7(1)	4745.8(3)
Z	4	4	4	4
Calc. Density (g·cm^{-3})	1.616	1.623	1.595	1.534
Absorption coefficient (mm^{-1})	2.197	2.206	11.111	1.913
Theta range for data collection (°)	1.8-35.7	2.1-32.9	3.3-70.4	1.5-30.6
Reflections collected	115603	159374	37407	169605
Independent reflections	18888	16609	9170	14355
R(int)	0.028	0.034	0.033	0.044
Data/restraints/parameters	17290/0/596	15792/0/596	8868/0/596	9542/1/596
Goodness-of-fit	1.09	1.08	1.09	0.97
Refinement on	F	F	F	F^2
Final *R* indices [$I > n\sigma(I)$]	0.0150 (n=3)	0.0125 (n=3)	0.0192 (n=3)	0.0163 (n=2)
Final w*R* indices [$I > n\sigma(I)$]	0.0152 (n=3)	0.0131 (n=3)	0.0228 (n=3)	0.0433 (n=2)
Flack parameter, nb Friedel-pairs	-0.015(2), 8300	-0.009(2), 7333	-0.0135(8), 4090	-0.014(2), 6445
Largest diff. Peak and hole (e Å^{-3})	0.97/-0.91	0.45/-0.46	3.31/-2.99	0.38/-0.19
CCDC reference number	2007105	2007104	2018680	2033959

Figure S1. Asymmetric units for Λ-**Dy** and Δ-**Dy** with numbering scheme.

[L^{Me2}Zn(Cl)Ln((*+*)-camph)$_2$(MeOH)], **Λ-Dy**	[L^{Me2}Zn(Cl)Ln((*-*)-camph)$_2$(MeOH)], **Δ-Dy**

ORTEP view (with ellipsoids at the 50%level of probability) of the asymmetric unit

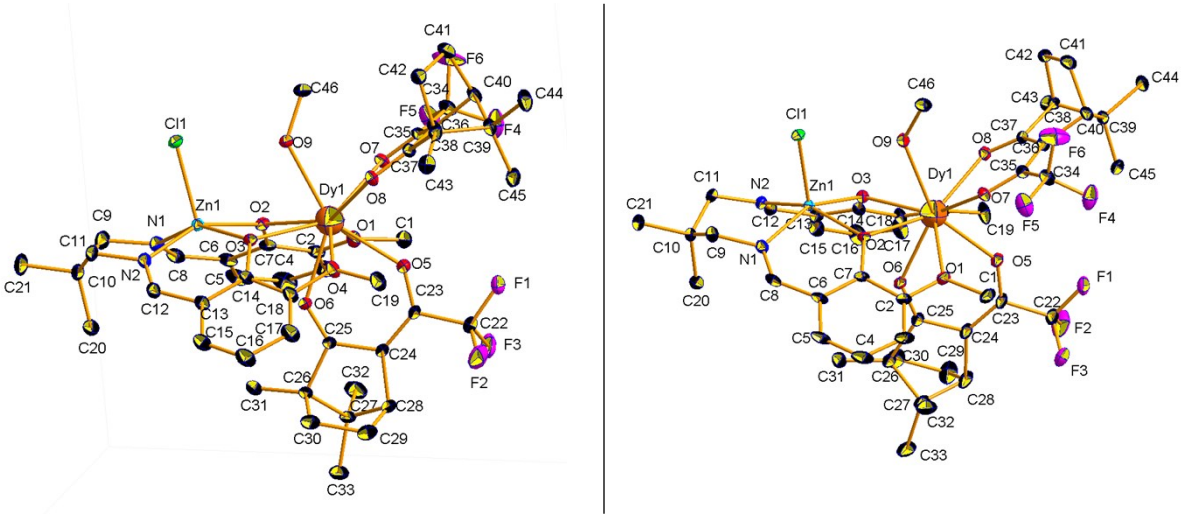

view illustrating the mirror-image relationship of the complexes.

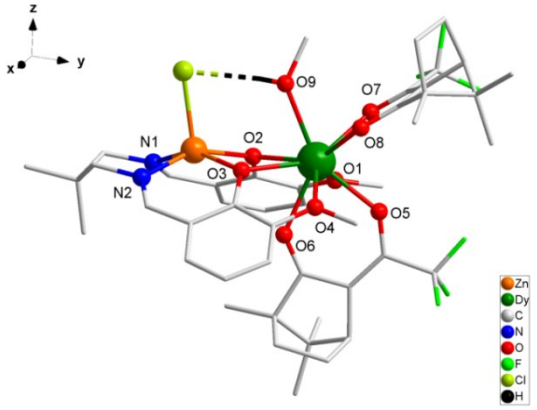

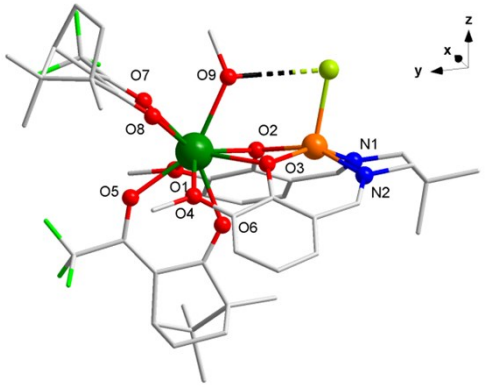

Figure S2. Λ-**Eu** : ORTEP plot (with ellipsoids at the 50% level of probability) of the asymmetric unit with numbering scheme.

[L^{Me2}Zn(Cl)Eu(*(+)*-camph)$_2$(MeOH)], **Λ-Eu**

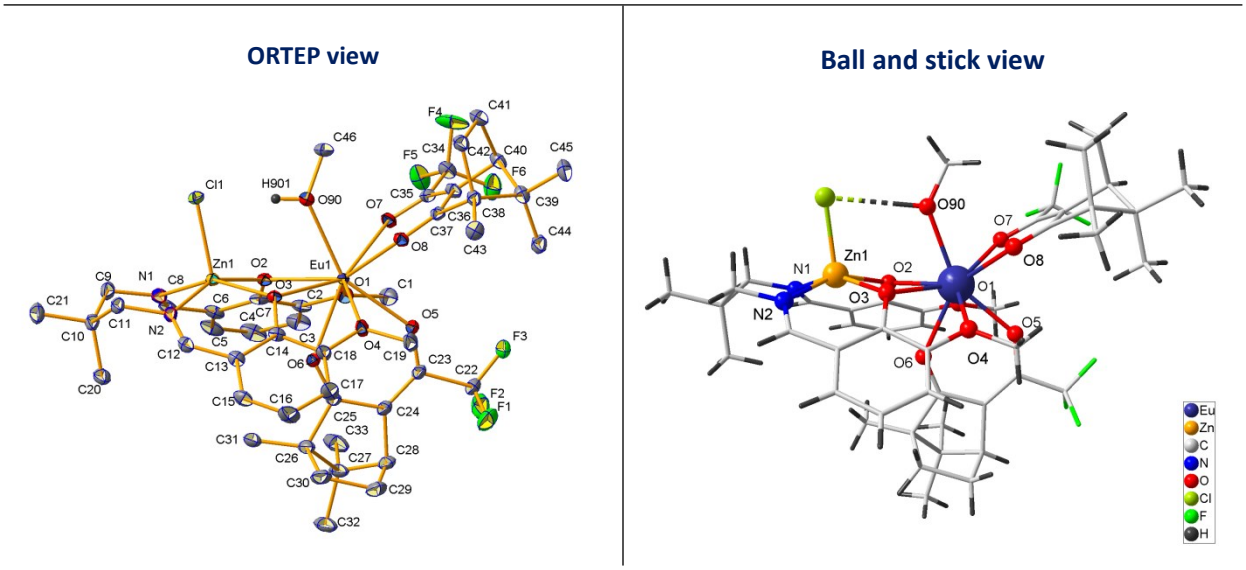

Figure S3. Λ-**Dy/Y** : ORTEP plot (with ellipsoids at the 50% level of probability) of the asymmetric unit with numbering scheme.

[L^{Me2}Zn(Cl)Dy/Y(*(+)*-camph)$_2$(MeOH)], **Λ-Dy/Y**

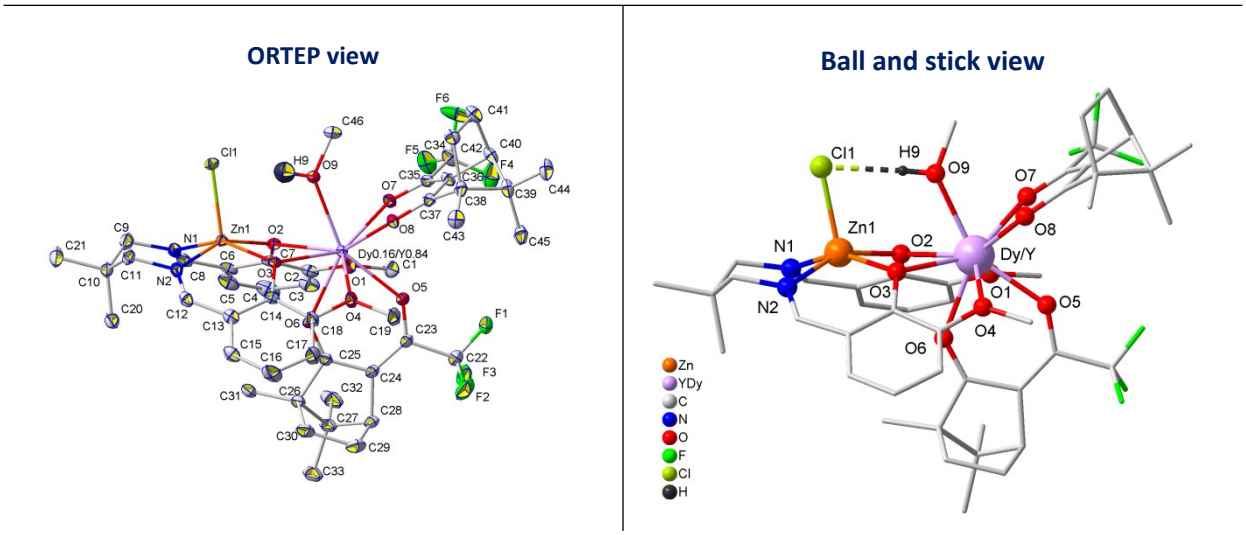

Table S2. Selected bond distances (Å) and angles (°) for **Δ-** and **Λ-Dy**, **Λ-Eu**, and **Λ-Dy/Y** complexes.

			Λ-Dy	**Δ-Dy**	**Λ-Eu**	**Λ-Dy/Y**
Zn1	N2		2.071(1)	2.0674(9)	2.068(2)	2.067(1)
	O2		2.0813(8)	2.0773(8)	2.081(1)	2.080(1)
	N1		2.086(1)	2.084(1)	2.0875(2)	2.086(1)
	O3		2.0907(8)	2.0904(6)	2.091(1)	2.091(1)
	Cl1		2.3116(3)	2.3091(3)	2.3077(5)	2.3087(4)
Dy1	O5		2.323(1)	2.3214(8)	2.352(1)	2.308(1)
	O7		2.3362(9)	2.3314(8)	2.378(1)	2.324(1)
	O6		2.3556(8)	2.3529(8)	2.395(1)	2.350(1)
	O2		2.4069(8)	2.4038(8)	2.438(1)	2.395(1)
	O8		2.407(1)	2.4063(8)	2.447(1)	2.356(1)
	O3		2.4243(8)	2.4231(6)	2.4565(1)	2.4114(9
	O9		2.440(1)	2.4375(8)	2.468(1)	2.420(1)
	O4		2.5370(9)	2.5330(8)	2.550 (1)	2.524(1)
	O1		2.5583(9)	2.5536(8)	2.568(1)	2.548(1)
C1	O1		1.435(2)	1.433(2)	1.435(2)	1.434(2)
C2	O1		1.374(2)	1.373(1)	1.377(3)	1.381(2)
C7	O2		1.326(1)	1.324(1)	1.327(2)	1.328(2)
C14	O3		1.325(1)	1.322(1)	1.324(2)	1.325(2)
C18	O4		1.375(2)	1.375(1)	1.377(2)	1.380(2)
C19	O4		1.438(2)	1.436(1)	1.439(2)	1.442(2)
C23	O5		1.280(2)	1.280(1)	1.277(2)	1.281(2)
C25	O6		1.242(1)	1.238(1)	1.239(2)	1.239(2)
C35	O7		1.273(2)	1.274(1)	1.274(2)	1.276(2)
C37	O8		1.246(2)	1.245(1)	1.244(2)	1.245(2)
C46	O9		1.431(2)	1.428(1)	1.432(2)	1.429(2)
Cl1	O9		3.022(1)	3.0219(8)	3.025(1)	3.022(1)
Cl1	H9		2.2273(3)	2.1898(3)	2.1764(4)	2.1600(4)
O2	Zn1	O3	80.49(3)	67.77(3)	80.95(5)	80.22(4)
O2	Dy1	O3	80.49(3)	67.83(3)	67.20(4)	67.98(3)

Table S3: SHAPE Analysis for the ML9 coordination sphere of the Ln ions.[1]

CSAPR-9	Spherical capped square antiprism
MFF-9	Muffin

[ML9]	CSAPR-9 (C_{4v})	MFF-9 (Cs)
Δ-Dy	1.396	**1.391**
Λ-Dy	1.399	**1.398**
Λ-Dy/Y	**1.356**	1.357
Λ-Eu	1.545	**1.457**

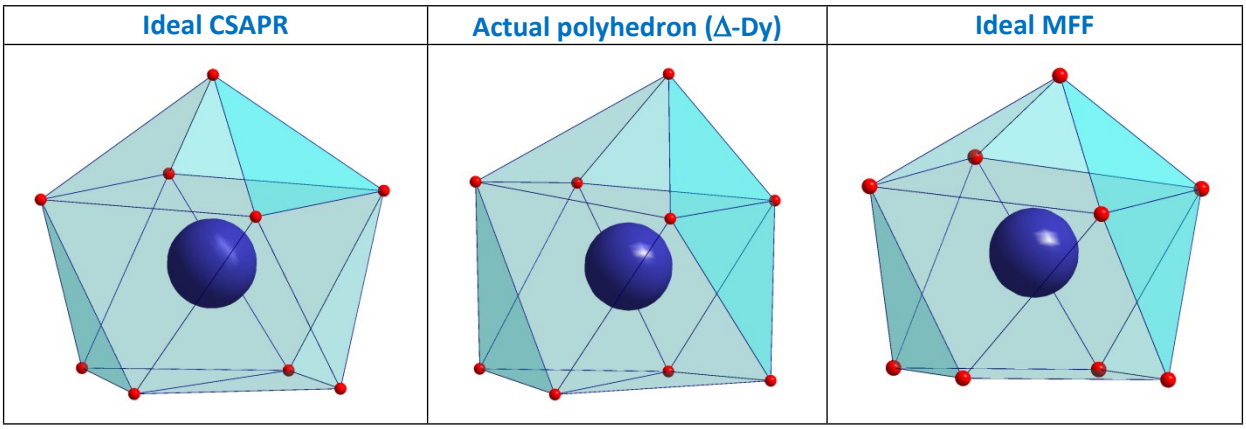

Figure S4. Solid-state UV-vis spectra for ZnL^{Me2} and $[L^{Me2}Zn(Cl)Dy((+/-)\text{-camph})_2(MeOH)]$ complexes.

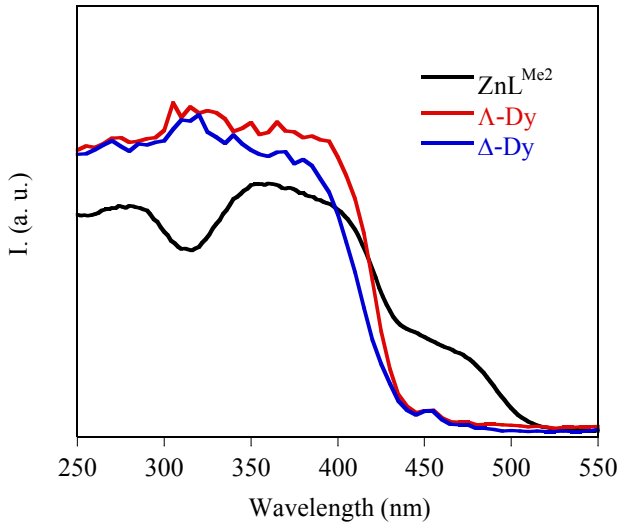

[1] Llunell, M.; Casanova, D.; Cirera, J.; Alemany, P.; Alvarez, S.; SHAPE: Program for the stereochemical analysis of molecular fragments by means of continuous shape measures and associated tools 2.1 ed.; University of Barcelona: Barcelona, 2013.

Figure S5. Magnetic behaviors for **Dy** complex.

Magnetic behavior is independent of the chirality therefore a full set of magnetic behavior has been collected only for **Λ-Dy**. The magnetic purity of the Δ enantiomer was confirmed by susceptibility values at 300 K (found $\chi_M T$ = 14.10 $cm^3mol^{-1}K$) and AC versus *T* trace with frequency of 1 kHz (shown below) that was found identical to **Λ-Dy**.

DC studies: The temperature dependence of $\chi_M T$ for **Λ-Dy** (Fig. S5a) is in agreement with the behavior expected for an isolated Dy(III) ion. The value found at 300 K is 14.15 $cm^3mol^{-1}K$ and reaches 11.41 $cm^3mol^{-1}K$ at 4 K. Magnetization versus field at 2 K (b) reaches as value of 5.35 μ_B under 5 T.

(a)

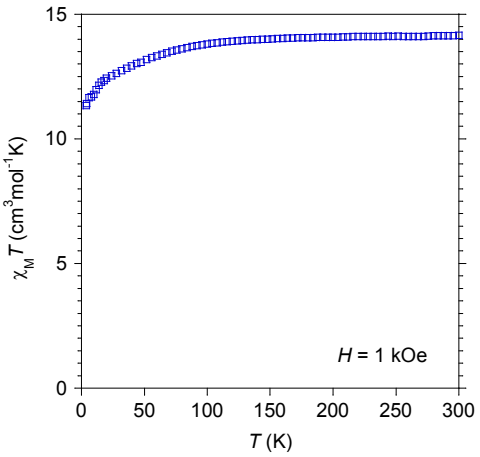

(b)

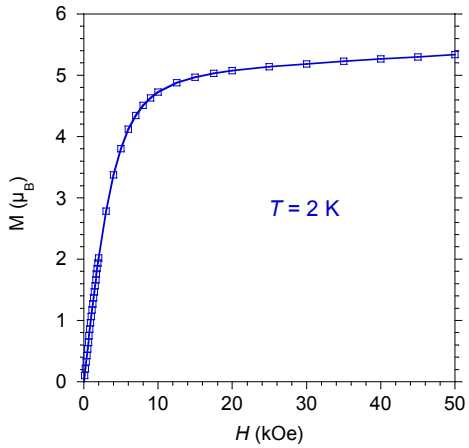

AC studies: AC magnetic susceptibility as a function of temperature recorded without an applied filed is shown in (c). An out-of-phase component, χ_M'', was found below 15 K and lower temperature behavior indicated other relaxation processes become active. Application of an external DC field allowed to drastically reduce these contributions but not to fully cancel them even when a field of 3 kOe (d). Since the $\chi_M'' = f(T)$ for different AC frequencies obtained with H_{DC} = 1 kOe display well defined maxima, a full data set was collected (e). The temperature dependence of the relaxation time between 3.8 and 10 K (f) was obtained by analyzing the $\chi_M'' = f(\nu)$ for different temperatures with an extended Debye model. The linear variation of $\tau = f(1/T)$ between 10 and 6.5 K was fitted assuming a thermally activated process yielding U_{eff}/k_B = 42 K with $\tau_0 = 1.4 \times 10^{-6}$ s (dotted blue line). A modelling over the entire temperature range (3.8 to 10 K, red line) was possible considering contributions from the Orbach and Raman relaxation processes ($\tau = \tau_0 e^{Ueff/kT} + 1/(RT^n)$). The values of the adjustment parameters are U_{eff}/k_B = 53 ± 9 K, $\tau_0 = 0.8 \pm 2 \times 10^{-8}$ s, R = 0.2 ± 0.1 s^{-1}, n = 4.9± 0.4.

(c)

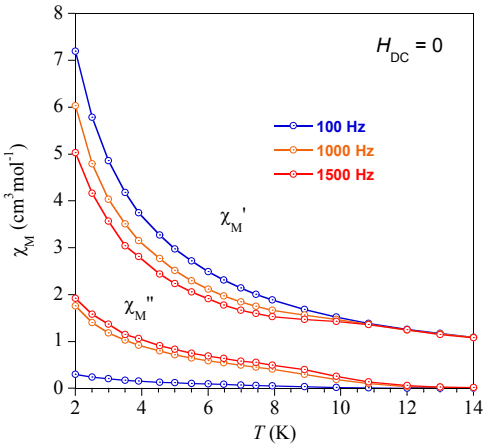

(d)

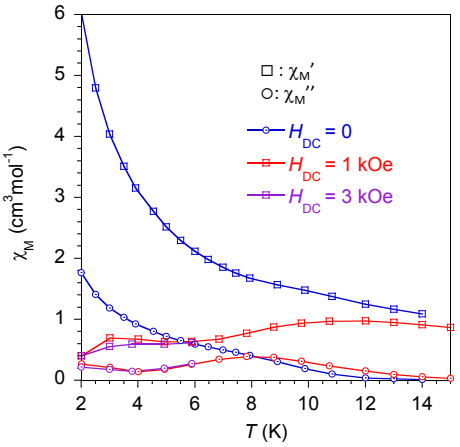

(e)

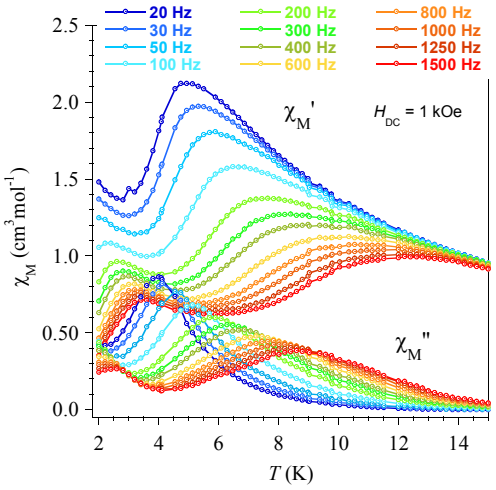

(f)

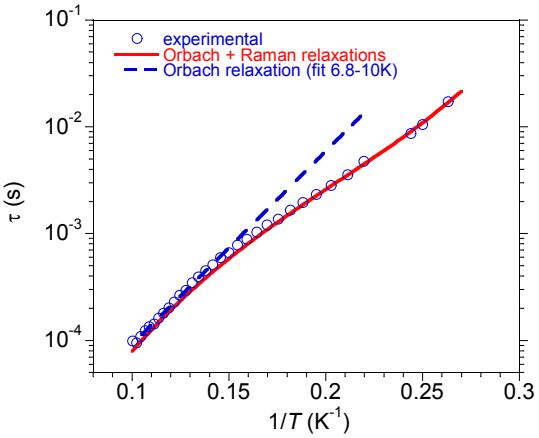

Figure S5g shows the χ_M'' = *f*(T) trace for **Δ-Dy** under H_{DC} = 1 kOe and for ν = 1 kHz which confirms a behavior identical to that of the Λ-Dy enantiomer.

(g)

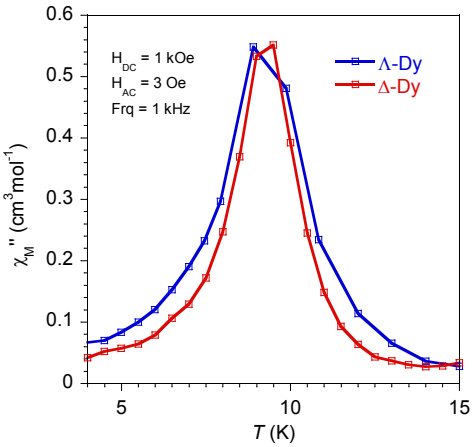

Figure S6. Magnetic behaviors for [L^{Me2}Zn(Cl)Y/Dy(*(+)*-camph)$_2$(MeOH)], **Λ-Dy/Y**.

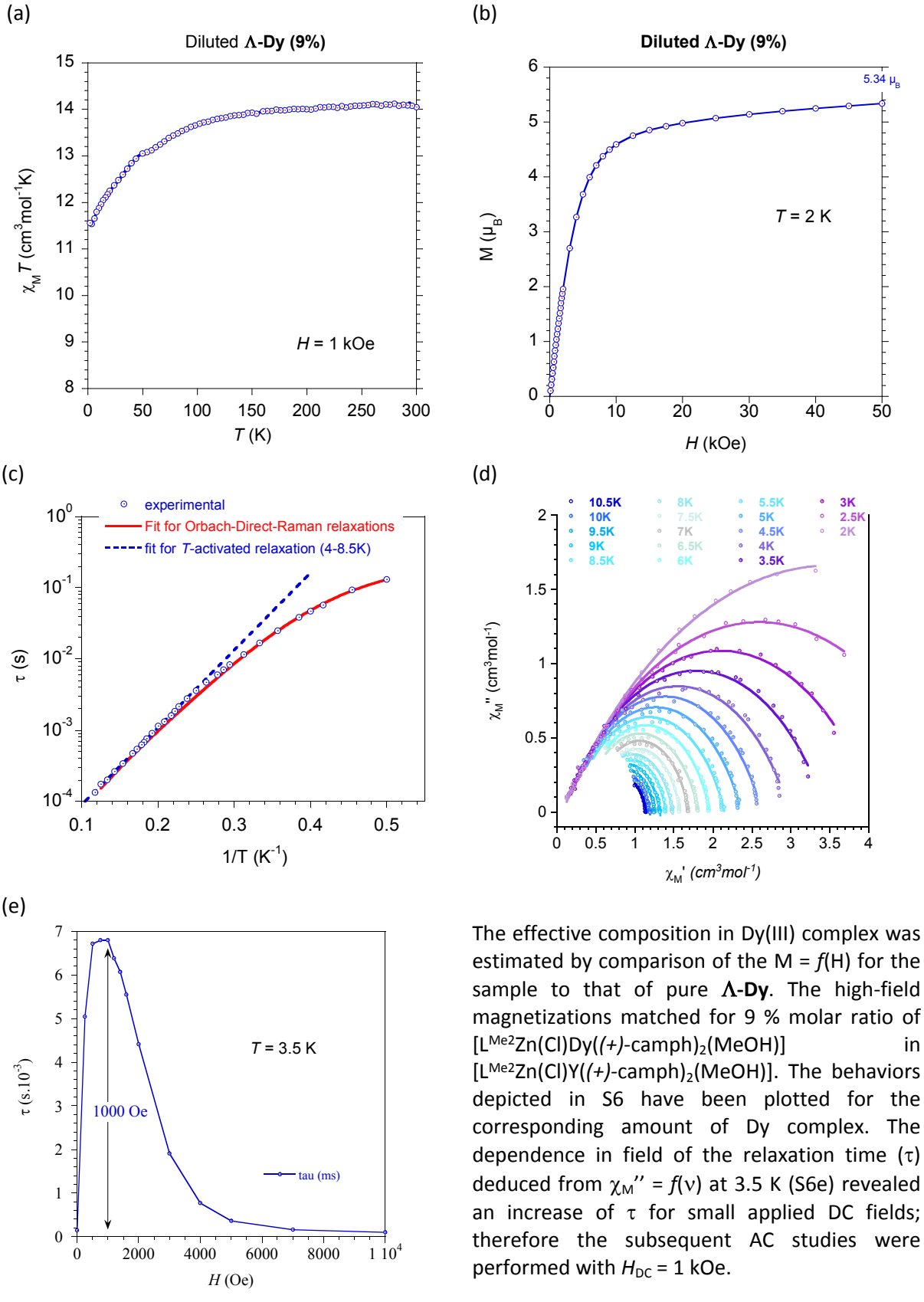

The effective composition in Dy(III) complex was estimated by comparison of the M = *f*(H) for the sample to that of pure **Λ-Dy**. The high-field magnetizations matched for 9 % molar ratio of [L^{Me2}Zn(Cl)Dy(*(+)*-camph)$_2$(MeOH)] in [L^{Me2}Zn(Cl)Y(*(+)*-camph)$_2$(MeOH)]. The behaviors depicted in S6 have been plotted for the corresponding amount of Dy complex. The dependence in field of the relaxation time (τ) deduced from χ_M'' = *f*(ν) at 3.5 K (S6e) revealed an increase of τ for small applied DC fields; therefore the subsequent AC studies were performed with H_{DC} = 1 kOe.

Picture 2: Crystals (size 300-800 µm) and powders (crushed crystal) on the cold stage for micro-photoluminescence studies.

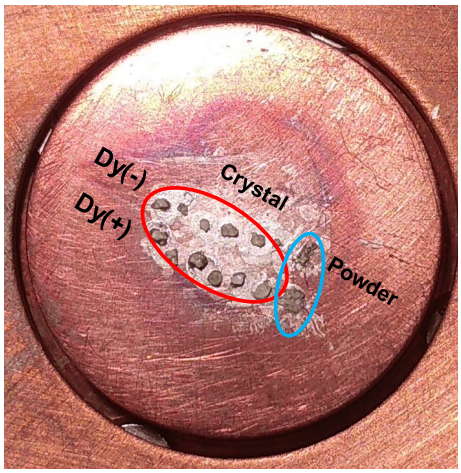

Figure S7. (a) Temperature dependent emission of a **Δ-Dy** crystal. Blue lines: left-handed circular (LHC) polarization; red lines: right-handed circular (RHL) polarization. (b) Temperature dependence of the deduced dissymmetry factor g_{lum}.

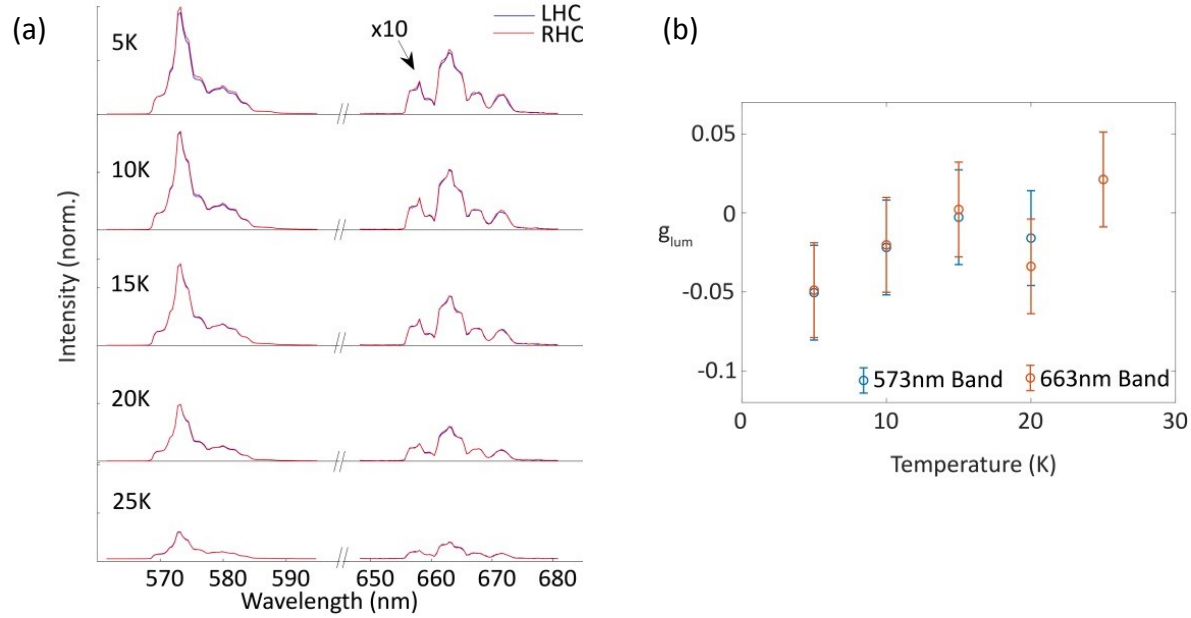

Figure S8. Temperature dependent emission and g_{lum} for a **Λ-Eu** (a, b), and a **Δ-Eu** (c, d) crystal (blue lines: left-handed circular (LHC) polarization; red lines: right-handed circular (RHL) polarization); (e) emission spectrum at 5 K (**Δ-Eu**).

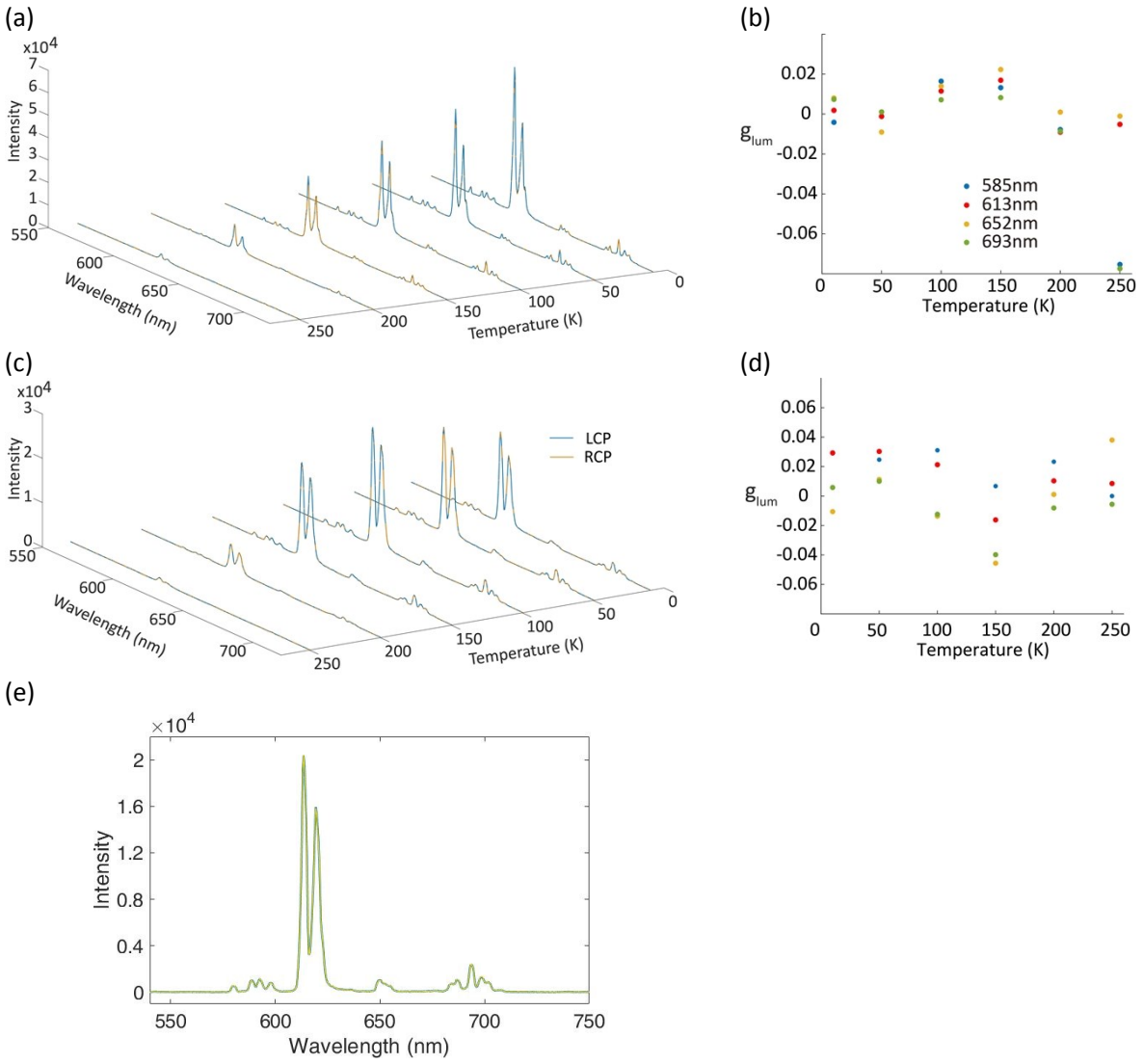

Figure S9. Angular distribution of the emission (bands at 573-nm and 663-nm) recorded at 5K, and temperature dependent variation of the dissymmetry factor g_{lum} for a crystalline powder of *(left)* **Λ-Dy** and *(right)* a **Δ-Dy** crystal. The grey portions correspond to the angles not collected by the objective (outside the numerical aperture).

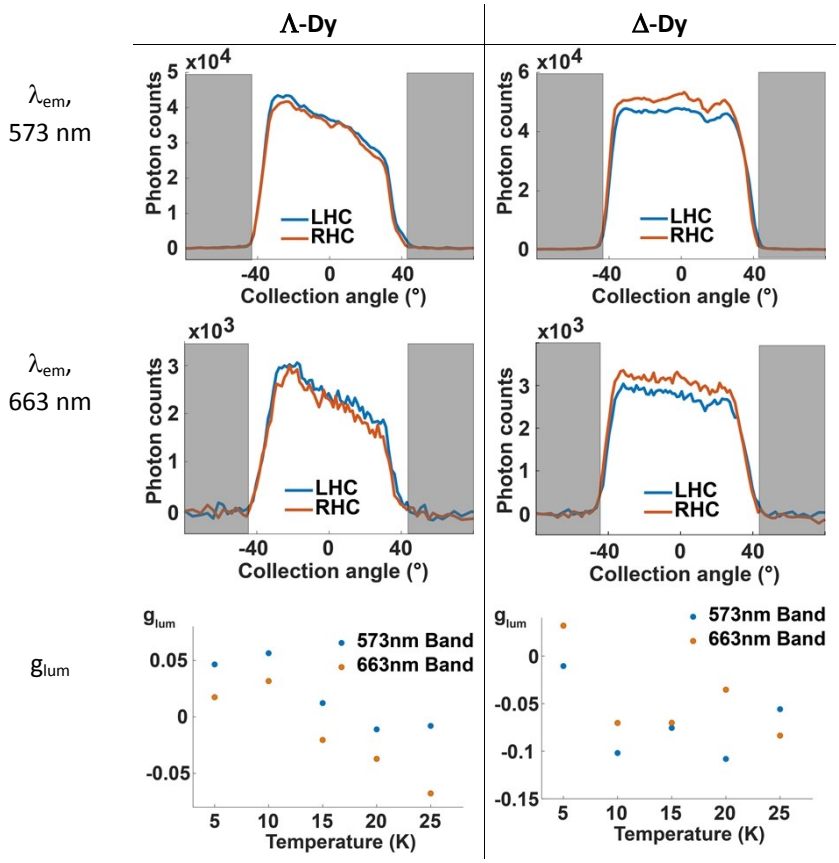

Figure S10. X-Ray Powder Diffraction (*XRPD*) at 295 K for **Λ-Dy** , **Δ-Dy**, **Λ-Eu**, and **Δ-Eu.**